Discover Nano

Research

Antimicrobial membranes based on polycaprolactone:pectin blends reinforced with zeolite faujasite for cloxacillin-controlled release

Bárbara Bernardi[1,2] · João Otávio Donizette Malafatti[1] · Ailton José Moreira[3] · Andressa Cristina de Almeida Nascimento[1,2] · Juliana Bruzaca Lima[3] · Lilian Aparecida Fiorini Vermeersch[1] · Elaine Cristina Paris[1]

Received: 30 August 2024 / Accepted: 2 December 2024
Published online: 14 January 2025

Abstract
Multifunctional membranes applied to biomedical materials become attractive to support the biological agents and increase their properties. In this study, biopolymeric fibers based on polycaprolactone (PCL) and pectin (PEC) were reinforced with faujasite zeolite (FAU) for cloxacillin antibiotic (CLX) loading. FAU with a high specific surface area (347 ± 8 m^2 g^{-1}), high crystallinity and particles with a diameter of up to 100 nm were produced under optimized synthesis conditions (100 °C/4 h). Zeolites were incorporated into polymeric nanofibers to be a cloxacillin (CLX) carrier in wound treatment, using electrospinning as an efficient synthesis method. The fibers produced showed good mechanical resistance and the incorporation of CLX was proven by assays to inhibit the growth of *Staphylococcus aureus* bacteria. The controlled release of CLX in different pH conditions, which simulate the wound environment, was carried out for up to 229 h, achieving a released CLX concentration of up to 6.18 ± 0.02 mg L^{-1}. These results prove that obtaining a hybrid fiber (polymer-zeolite) to incorporate drugs to be released in a controlled manner was successfully achieved. The bactericidal activity of this material shows that its use for measured applications could be an alternative to conventional methods.

Keywords Antimicrobial · Electrospun · Nanofibers · Pectin · Faujasite · Polycaprolactone

1 Introduction

Wound dressings are part of biomedical materials essential to skin infections, acting as external barrier protection (physical, chemical, and biological) and drug release systems [1]. Bactericidal dressings have the advantages of non-invasive administration, protection against external entry of harmful microorganisms, and easy application [2]. Furthermore, encapsulate administrations can minimize the drug excess when applied directly to the skin, releasing control [3, 4]. This way, modulating the result is possible from the best performance in the therapeutic window due to the excreted fraction, avoiding high concentration in the bloodstream, which results in toxicity [5, 6]. The efficiency depends on dermal compatibility, good fixation, mechanical flexibility, and the ability to encapsulate biological agents for release [7, 8].

Polymeric fiber membranes are an excellent alternative to matrix dressing, increasing the surface area, porosity, and versatility, promoting a favorable drug incorporating and posterior release, and dressing more significant contact with the infected area [9–11]. Controlled release minimizes the toxicity due to high doses of application, as well as eliminating

✉ Elaine Cristina Paris, elaine.paris@embrapa.br | [1]National Nanotechnology Laboratory for Agriculture (LNNA), Embrapa Instrumentação, 1452 XV de Novembro St., São Carlos, SP 13560-970, Brazil. [2]Department of Chemistry, Federal University of São Carlos, Rod. Washington Luís, Km 235, São Carlos, SP 13565-905, Brazil. [3]Institute of Chemistry, São Paulo State University (UNESP), Araraquara, SP 14800-060, Brazil.

the inconvenience of continuous invasive application. However, producing polymeric membranes with such properties is a major challenge that requires new synthetic routes to achieve a chemical composition that guarantees stability for the application and compatibility with the cell structure [12]. The electrospinning method is a technique that allows the transformation of a variety of polymers into fibers with controlled morphology and composition [12–14]. The fibers obtained through this technique have proven to be efficient in encapsulating drugs and maintaining an environment for the regeneration of the biological system, making them attractive for producing materials that improve the treatment of wounds and infected areas [2, 10].

Biocompatible polymers such as polyvinyl alcohol (PVA), polylactic acid (PLA), and polycaprolactone (PCL) support a range of antimicrobial agents against bacteria, fungi, and viruses associated with different diseases [15]. Additionally, biologically compatible, biodegradable, and low-cost products are desirable for these dressings, minimizing the environmental impact and production costs [16, 17]. Polycaprolactone (PCL) is a polyester synthetic polymer with elastic, biodegradable, and hydrophobic characteristics approved by the United States Food and Drug Administration (FDA). In biomedical applications, PCL fiber membranes have demonstrated the capacity to increase drug encapsulation and microbial control [12, 18]. On the other hand, pectin (PEC) is a polymer with glycosidic bonds, many branches, and hydroxyl groups, which gives it a hydrophilic character and hydrocolloid properties [18, 19]. Other advantages of their use are low cost, renewable, biocompatible, and high availability. Combining polymers has advantages for these membranes, improving the type of drugs incorporated, behavior release, adhesion skin, and permeability by adding other carrier agents [20–22]. Studies involving the combination of polymers with different characteristics can overcome these limitations and lead to a superior medical treatment [23]. In particular, the PCL:PEC (PP) blend proposal for wound dressing is an interesting material for evaluating miscibility and compatibility.

Polymeric fiber membranes with the addition of particulates (ceramics, polymers, etc.) show advantageous characteristics for dressing production, exhibiting improvement since mechanical properties and external barrier [24–27]. The presence of active particles between the chain polymeric help to absorb the tension traction and increase sites in the membrane that are available to electrostatic interaction, covalent bonds, and others. The usual reinforcement materials are as nanocellulose [28], general oxides [29], clays [12], silicates [30], and zeolites [31] are examples of biomedical materials applications. Zeolites are aluminosilicates with tridimensional structures that are porous, chemically stable, and biocompatible [32, 33]. In particular, Faujasite (FAU) is one zeolite family with high surface area and efficient dispersibility, allowing homogeneous distribution and more effective reinforcement properties [34]. In addition to these characteristics, FAU zeolite's biocompatibility and stability in biological environments (carrier agent and target molecule affinity) make it an exciting material for biological applications [34, 35]. In this context, using FAU can be a promising way to improve the resistance traction of the fiber membranes based on the present work on PCL:PEC:FAU (PPF) turning more efficient to a wound dressing.

Polymeric fiber membranes with the addition of particulates (ceramics, polymers, etc.) show advantageous characteristics for dressing production, exhibiting improvement since mechanical properties and external barriers are examples in biomedical applications [36]. Zeolites are aluminosilicates with tridimensional structures, porous, chemically stable, and biocompatible. Faujasite (FAU) is one zeolite family with high surface area and good dispersibility, allowing homogeneous distribution efficiency and more effective reinforcement properties. In addition to these characteristics, FAU zeolite's biocompatibility and stability in biological environments (carrier agent and target molecule affinity) make it an exciting material for biological applications. Polymeric blends containing 3D ceramic structures as drug carriers requires well-controlled synthesis methods. In this context, using FAU can be a promising way to improve the resistance traction of the fiber membranes based on the present work on PCL:PEC:FAU (PPF) turning efficient to wound dressing.

The literature [37, 38] on biomedical materials has recently increased from dressing healing to surgical improvement applications. The system PCL:PEC:FAU (PPF) is not entirely reported in the literature [39–41], including fiber membranes, drug release, and antimicrobial activity. The production of a mixture of PCL:PEC polymers to incorporate the FAU zeolite as a drug carrier, stable during release and biodegradable afterward, is a proposal applicable in the health application. Furthermore, if it is proven that the incorporation of the drug into the fiber is effective, the material could also be applied in bactericidal activity studies [42, 43]. A search of the literature did not find other studies with this material composition with the goal for the immobilization of drugs. Thus, the present work studied the affinity of polycaprolactone and pectin to form fibers and the effect of zeolite insertion as mechanical reinforcement. *Staphylococcus aureus* (Gram-positive) inhibition assays were used to prove the bactericidal activity. *Staphylococcus spp* is one of the microorganisms responsible for various infections, skin diseases, and open wounds. The treatment is commonly based on the application of antibiotics such as cloxacillin, cephalexin, and others [44, 45]. In the present work, sodium cloxacillin (CLX) was used as a drug model and incorporated into wound dressing. Furthermore, CLX-controlled release studies were conducted using

different aqueous solutions and buffers simulating biological conditions. This way, the present work expects to contribute to the biomedical literature by exhibiting an alternative system to drug release and biological control.

2 Materials and methods

2.1 Faujasite zeolite (FAU) synthesis

Faujasite synthesis was based on the methodology of Meirelles et al. [46]. Initially, 3.52 g of sodium aluminate [Al_2O_3 (50–56%) Na_2O (37–45%) Sigma-Aldrich] was solubilized in 25 mL of deionized water under magnetic stirring at room temperature. Next, 10.85 g of sodium hydroxide (NaOH, 97%, Synth) solubilized in 25 mL water deionized was added into the sodium aluminate solution. In sequence, 50 mL of deionized water was added to complete the total volume. Next, 16.22 g of SiO_2 (Aerosil 380, Evonik) was continuously added into the reaction medium to obtain a gel. The gel was aged for 24 h under static and ambient conditions. Then, the gel was subjected to hydrothermal treatment at a heating rate of 3 °C min^{-1} up to 100 °C for 3 h.

2.2 Polycaprolactone: pectin (PP) fiber membranes

The methodology for producing PCL:PEC (PP) fibers was adapted from Malafatti et al. [47]. Initially, polycaprolactone (PCL, 50,000 MW, Perstorp) was solubilized in chloroform (99.8%, Synth), with posterior addition of dimethyl sulfoxide (DMSO, 99.9%, Synth). PCL was added to obtain a 10% (w w^{-1}) of total volume and ratio of solvents chloroform:DMSO corresponding to 4:1 (v v^{-1}). For PP blends, pectin (PEC, Genu USP B—CPKelco) was dispersed in previous agitation for 30 min in DMSO solvent, being mixed with PCL solubilized in chloroform. Regarding the PCL weight, different proportions of PEC were evaluated from 0, 10, 20, 30, and 50% (w w^{-1}). The fibers were identified as PP X, being X an amount percentual added in the initial polymeric solution.

The electrospinning system consists of a Glassman High Voltage brand Glassman High Voltage, model PS/FC60P02.0–22, an ejector pump of the KVS model 100 ejector pump, a 20 mL Art Glass syringe, and 40 × 1.2 mm needle. In an electrospinning system, the polymer solution, previously prepared, is inserted into a syringe that is coupled to a metal needle connected to a high-voltage source. The ejector pump is responsible for forcing the polymer solution out through the orifice of the needle. In this process, the polymer solution is pushed out of the syringe, forming a drop, deformed to form a Taylor cone. When the applied tension exceeds the droplet's surface tension, a jet of the polymer solution is ejected, causing the polymer to stretch and the solvent to evaporate [48]. This fiber polymeric is collected in the (grounded) metalic collector under 180 rpm rotation to cover the entire surface and was set up so that the needle was fixed at 10 cm from the cylindrical metal collector covered with aluminum foil. The fibers were electrospinning until the precursor solution in the syringe was completely consumed using a flow of 1.2 mL h^{-1} and a voltage of 20 kV. After electrospinning, the fibers were collected from the foil.

2.3 PCL:PEC:FAU fibers (PPF) membranes

The PCL:PEC:FAU (PPF) nanocomposite fibers were performed using the PP 10, corresponding to 10% (w w^{-1}) PEC. Concerning PCL weight, FAU zeolite (2.5% w w^{-1}) was added to the PP precursor solution. After adding the FAU, the solution was kept stirring for 1 h. Electrospinning was then carried out under the same conditions described in item 2.2. The sample was identified as PPF.

2.4 Cloxacillin (CLX) incorporated into PPF membranes

The insertion of sodium cloxacillin (CLX, INLAB) was evaluated using PCL pure fibers, PP 10 blend, and PPF nanocomposite. The procedure consisted of 20% (w w^{-1}) of PCL weight in polymeric solution solubilized and homogeneized. The mixture was kept stirring for 1 h until the CLX was solubilized. Then, the fibers were electrospun using the conditions described in item 2.2. The samples were identified as PCLCLX, PPCLX, and PPFCLX.

2.5 Materials characterization

X-ray diffraction analysis was carried out on Shimadzu® equipment, model LabX XRD-6000, using Cu-Kα radiation of λ = 1.5406 Å. The scan was performed continuously at 1° min^{-1} with 2θ ranging from 5 to 50º. The adsorption/desorption N_2 analysis using the Brunauer–Emmett–Teller (BET) method was carried out on the ASAP 2020 equipment (Micrometrics). Previously, 100 mg of the sample was pre-treated at 100ºC under a pressure of 10 µmHg. The Zeta Potential was performed at the Malvern Instruments—Zetasizer Nano ZS90. The measurements used 1 mg of zeolite dispersed in 15 mL of deionized water and sonicated in a tip ultrasound for 20 s, at 5 s intervals, with an amplitude of 20%. The measurements were made in triplicate. The FTIR (Fourier Transformed Infrared Spectroscopy) analyses were carried out on Bruker equipment (Vertex 70) using the ATR (Attenuated Total Reflectance) mode. The spectra were generated with 32 scans from 4000 to 400 cm^{-1} and a resolution of 4 cm^{-1}.

The morphology of the fibers and particles was analyzed using a scanning electron microscope (SEM, JEOL 6510). For the fibers, squares of approximately 5 mm^2 in area were applied to a carbon tape on a metal stub. The samples were then coated with gold using a Leica SCD 050 metallizer. FAU particles were deposited directly on the carbon tape in a metal stub, and then an air flow was used to remove the loose particles without needing metal coating. A DMA Q800 V21.3 Build 96 equipment was used for the mechanical tensile test. The measurements were taken by applying the clamp module and varying the traction force by 1 N s^{-1} until the membrane broke. In this analysis, rectangular specimens measuring 6.32 × 18.48 mm were used, with the thickness varying according to the deposition of the fibers during the electrospinning process. Thermogravimetric (TG) analysis was performed on a TA instrument (Q500 Series), and 6 to 10 mg of each sample was previously dried in an oven. The samples were then analyzed under a flow of 40 mL min^{-1} of N_2 and 60 mL min^{-1} of synthetic air, a heating rate of 10 °C min^{-1} in a temperature range between 40 and 700 °C. The contact angle was measured on KSV Instruments equipment (CAM 101). Droplets with a volume of 3–5 µL of water were used to calculate the drop angle during 60 s deposition on the fiber.

2.6 Antimicrobial activity

The bactericidal activity of the mat fibers with the cloxacillin antibiotic was investigated by the disc diffusion method [12] using the microorganism *Staphylococcus aureus* (INCQS 15 ATCC 25923). Initially, a previous inoculum was prepared at 36 °C by adjusting the concentration to 1.10^6 cells using the McFarland scale using ultraviolet–visible spectroscopy (625 nm). In a Petri dish containing Müller-Hinton agar, 100 µL of this inoculated suspension was plated. Posterior, the materials of interest were deposited on a plate and incubated in an oven at 36 °C for 12 h. The test was performed on the FAU, antibiotic powders, and cut fiber discs (PCL, PCLCLX, PPF, and PPFCLX). After this period, the zone of bacterial growth inhibition was measured using a caliper (triplicate).

2.7 CLX release assays

PPFCLX (75 mg) was added to 250 mL of ultrapure water, 5 mmol L^{-1} phosphate buffer solution (pH = 5.5), or 5 mmol carbonate buffer solution. mmol L^{-1} (pH = 5.5). The experiments were kept at 37 °C, simulating body temperature, and mechanically stirred for up to 229 h. Aliquots (0–229 h) of the solution were collected. The CLX concentration was analyzed by high-performance liquid chromatography (HPLC) using Agilent equipment, 1260 Infinity II model, UV–VIS detector (205 nm), Poroshel 120 column, C-18, 4.6 × 100 mm, 4 µm, 40 °C. Separation was achieved using a 0.001% formic acid (AF, v v^{-1})/Acetonitrile (ACN) mobile phase at a flow rate of 0.8 mL min^{-1} in isocratic mode (50%AF:50%ACN). A calibration curve was constructed for the linear range of 0.1—10 mg L^{-1} from the pure CLX standard (99%, Sigma Aldrich). The limit of quantification (LOQ), the limit of detection (LOD), and the linear correlation coefficient (R^2) were LOQ = 0.292 mg L^{-1}, LOD = 0.087 mg L^{-1}, and R^2 = 0.999, respectively.

3 Results and discussion

3.1 FAU characterization

Figure 1a shows the X-ray diffractograms of the synthesized FAU and the silica precursor. SiO_2 (Aerosil 380) exhibits amorphous characteristics with a single broadband peak centered at 2ϴ 22.3°, typical for this material. The obtained zeolite

exhibits a diffractogram with profile peaks (2θ) corresponding to the formation of the FAU phase relative to pattern card JCPDS no 043–0168 [49]. The baseline definition and intensity of diffraction peaks demonstrate a monophasic FAU crystallinity. The absence of additional peaks indicates no secondary phases under this condition. This result corroborates what is reported in the literature [50–52]. Furthermore, it is essential to elucidate that the zeolite phase is influenced by the synthesis time, and even slight variations in the heat treatment became competitive with other zeolite structures [50, 53].

The crystallization of zeolites into structures with different dimensions is strongly related to the hydrothermal treatment time. This behavior occurs because the crystallization seeds can grow into small-diameter structures, dissolve again, and recrystallize into organized structures [54]. SEM analysis was performed to verify the morphology transformations, as shown in Fig. 1b. Image analysis shows that FAU zeolite has an increased dimension with particles agglomerate and polydisperse, ranging from 100 to 2500 nm.

Concerning surface properties, this FAU synthesized exhibited an external surface area of $347 \pm 8\ m^2\ g^{-1}$, $29 \pm 8\ m^2\ g^{-1}$ of specific surface area, and $318 \pm 8\ m^2\ g^{-1}$ of the pore area. These values reinforce the formation of the FAU zeolite. Thus, the obtained zeolite shows a porosity typical for this class material with range values with a three-dimensional pore structure characterized by a large area [55]. About the charge surface, the zeta potential (ζ) corresponds to—48 ± 2 mV. The negative value is explained by the deprotonation of siloxane groups in the zeolite structure, which is characteristic of the material, according to other reports in the literature [56]. This higher value is an essential property of this material about the external interaction and stability in suspension. Higher surface charge values promote a repulsion particle, reducing sedimentation by agglomerate formation. Thus, by adding FAU during the polymeric solution, this material could perform better, improving a homogeneous distribution and an excellent mechanical response.

3.2 PP and PPF fiber membranes

PP polymeric blends were analyzed by SEM analysis (Fig. 2), verifying the effect of pectin addition in the morphology. PCL pure membranes (Fig. 2a) showed fibers with 127 ± 52 nm diameter. The addition of PEC (10, 20, 30, and 50%) showed similar behavior to PCL pure fibers with efficient homogeneity with values of 147 ± 51 nm, 157 ± 79 nm, 155 ± 54 nm, and 131 ± 46 nm, respectively. Additionally, the materials showed efficient fiber formation, with tiny beads distributed in the overall structure. The beads are naturally present in polymer fibers due to the collapse of the polymer during fiber production [57]. In any case, the electrospinning fibers were successfully produced at all PP blends.

The thermal behavior of the PP fibers was performed by thermogravimetric analysis (TGA), verifying the effect of PEC addition, showed in Fig. 3. First are the mass loss events for PEC and PCL, as PEC is more susceptible to degradation at lower temperatures than PCL. For PEC, between 200 and 430 °C, a mass loss superior to 60% is observed for PEC, which can be associated with the degradation of the β pectin chain. The 200–250 °C event is attributed to the chemical bond breakage in the PEC cyclic structure [19]. A single transition event on PCL is confirmed between 350 and 400 °C, revealing its superior resistance to thermal degradation than PEC.

The PCL thermal degradation is associated with the molecule's bond breakage to produce gases and water and, consequently, the depolymerization of the molecular structure [21]. The PP fibers with different PEC concentrations showed thermal degradation behavior like PCL, even for the higher (30% PEC) [58]. For all PP blends, 10–50% PEC is verified around 420–450 °C a mass loss event (about 10%) in the same region observed for PEC. Additionally, increasing PEC percentual is not observed as a proportional mass loss. This result could be related to partial miscibility; only part of this polymer can interact with PCL to chain structural differences, corroborating the visual observation in the syringe during electrospinning (PEC decantation).

The partial miscibility of PCL and PEC can be relative to the opposite properties found in polymeric chains. PCL is a hydrophobic polymer due to its long carbon chain. At the same time, PEC is known to be hydrophilic, attributed to the

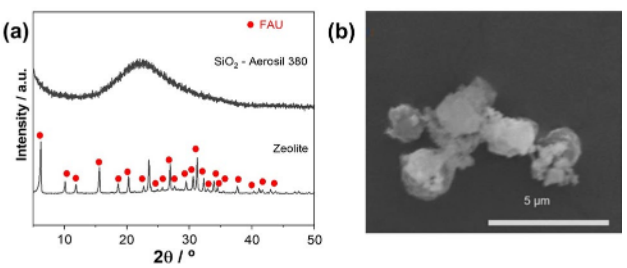

Fig. 1 **a** X-ray diffractogram (XDR) and **b** scanning electronic microscopy (SEM) image of the synthesized zeolite

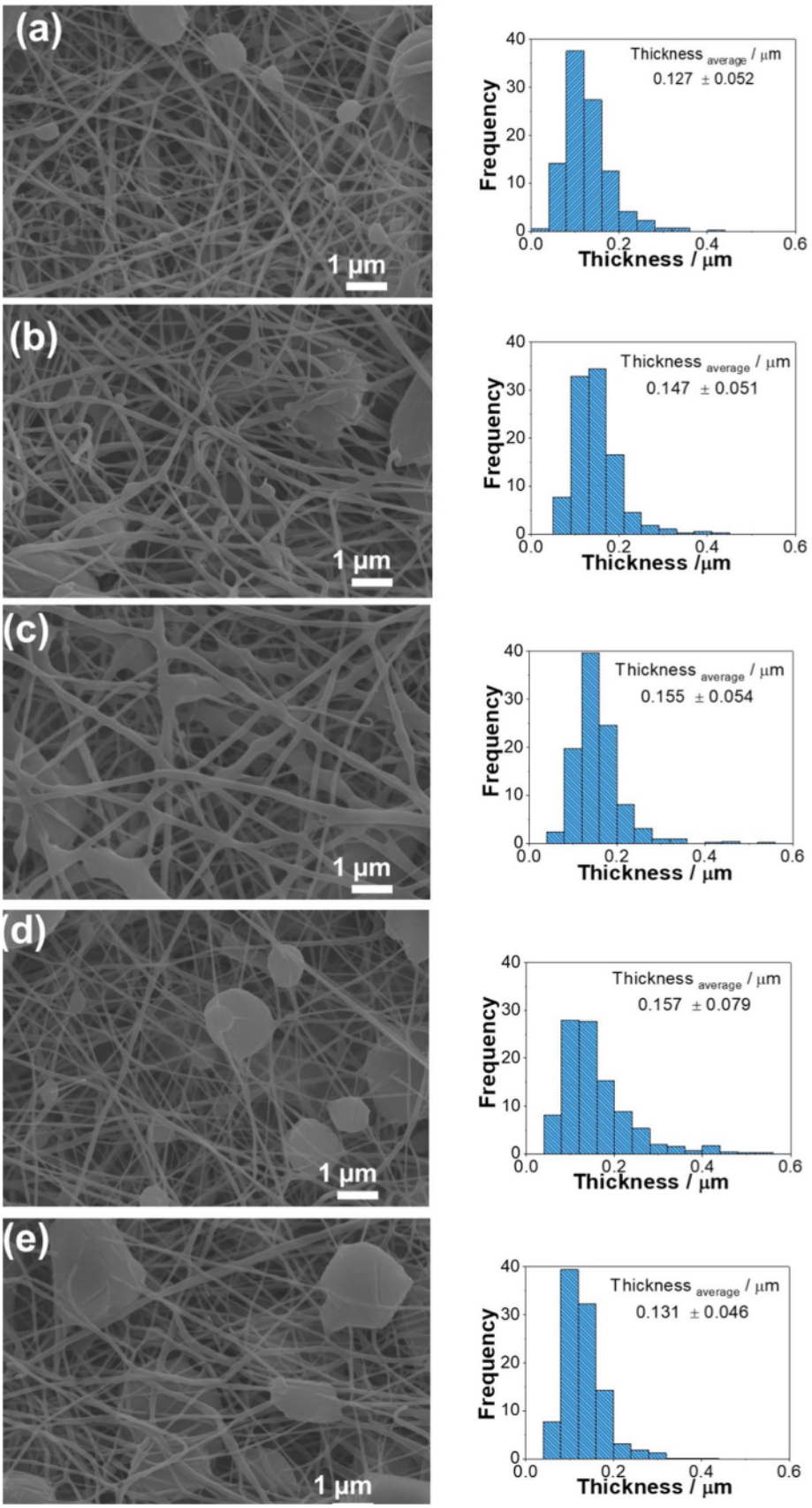

Fig. 2 SEM Images and diameter of the fibers: **a** PCL, **b** PP 10, **c** PP 20, **d** PP 30, and **e** PP 50

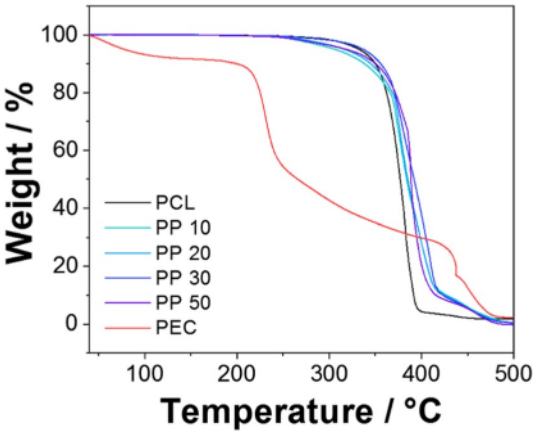

Fig. 3 Thermogravimetry analysis of PEC powder, PCL, and PP fibers

carboxylic and hydroxyl surface groups [7, 19]. Once both exhibit characteristics that can affect their barrier to external humidity and water affinity, the wettability assay performed for the PP fibers was also investigated in this study.

Figure 4 shows PP with all different PEC additions with a higher contact angle value against water, like PCL pure fibers. The PCL (126 ± 13°) showed the highest contact angle due to its elevated hydrophobicity. The fiber PP 10 showed an angle of 104 ± 5°, the maximum decrease, but with no statistical relevance. However, as expected, the PEC insertion in PP fibers did not promote the consecutive hydrophilicity increase. This result could be correlated in Fig. 3 by TGA analysis, which did not observe the significative mass loss relative to PEC with the polymer addition, indicating the effective increase of PEC in superior initial concentrations.

Furthermore, the simple mixture of PCL and PEC did not result in a progressive hydrophobicity or range of hydrophilicity. In this case, the PP 10 blend is the maximum additional to be incorporated into PCL, with predominant hydrophobic properties. In this case, a wound dressing with this property can act as an external barrier to humidity, essential to preserving the infection area against external contamination. It is important to emphasize that blending materials allows the control-release of different drugs into biological systems, external barriers, and adhesion skin, maximizing the combat against microbial infection [59].

PP 10 fiber membranes were chosen as the blend to be considered in this work once the TGA (Fig. 3) and contact angle (Fig. 4) showed that superior additions were not effectively inserted and did not favor their properties. The stability of a wounding dressing is essential to guarantee that the polymeric matrix maintains the desirable characteristics. In this case, PCL and PP 10 fibers were submitted to a swelling (Fig. 5) and degradability assay (Fig. 6) in a phosphate buffer solution (pH 5.5), simulating the pH of human skin. The test was performed for 60 days using gravimetric assays. Figure 5

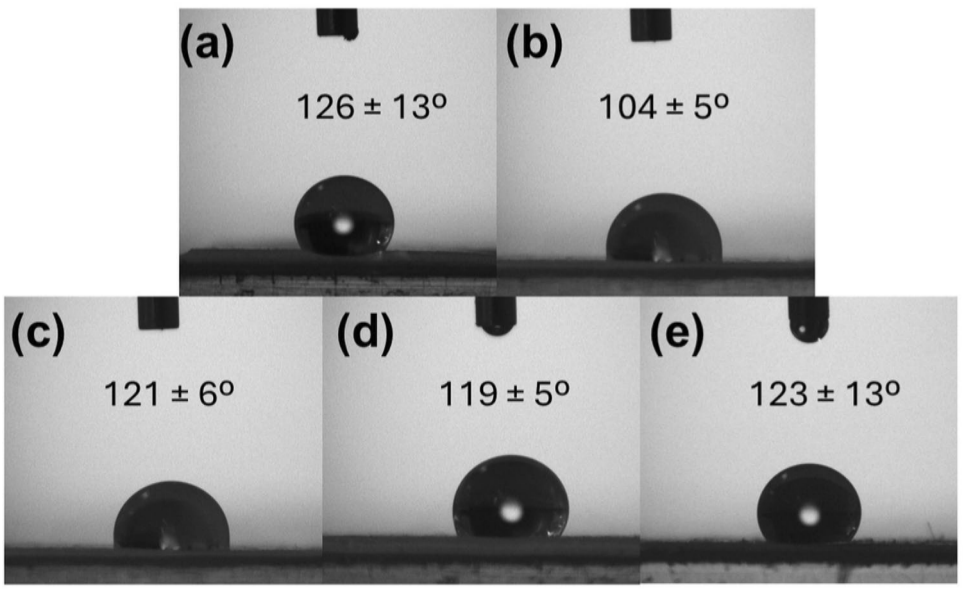

Fig. 4 Angle contact images of fibers **a** PCL, **b** PP 10, **c** PP 20. **d** PP 30, and **e** PP 50

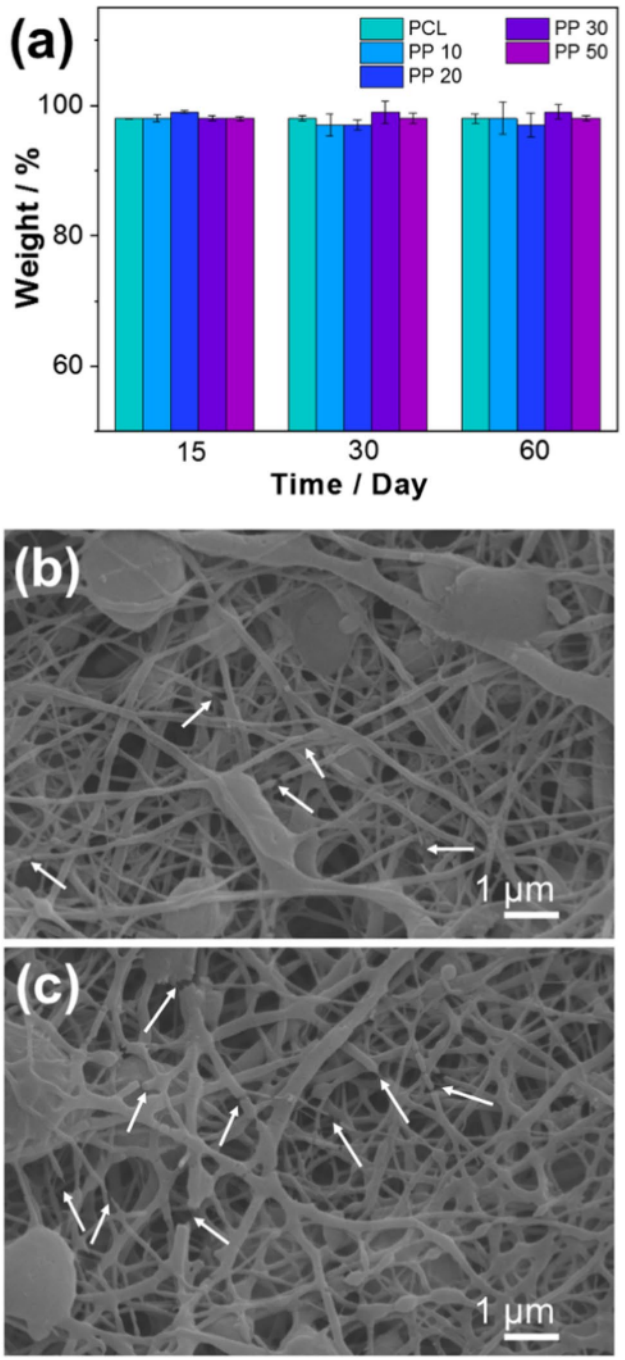

Fig. 5 **a** Wettability of PCL and PP fibers, **b** PCL, and **c** PP 10 after 60 days exposition in phosphate buffer pH 5.5

shows that the PCL and PP fiber membranes or the reinforced fibers with different percentages of PEC did not show any significant mass variation, even in more extended periods up to 60 days. This result correlates with the previous result (Fig. 4) that showed the lower water affinity water, leading to swelling membranes or their structure degradation.

SEM images were performed on PCL and PP 10, once this indicated the maximum that could be blended to check for possible interactions with an external medium. Breakpoints in structure fibers were found in both PCL and PP 10 after the end of the experiment (Fig. 5b, c). However, PP 10 (Fig. 5c) can observe more rupture points in the fiber structure. A possible association to the highest number of breaking points observed for PP 10 could be associated with PEC presence and their hydrophilic and acidity properties, favorably external interaction. This way, PP 10 demonstrated efficient structure stability for a possible membrane to be applied as a wound dressing.

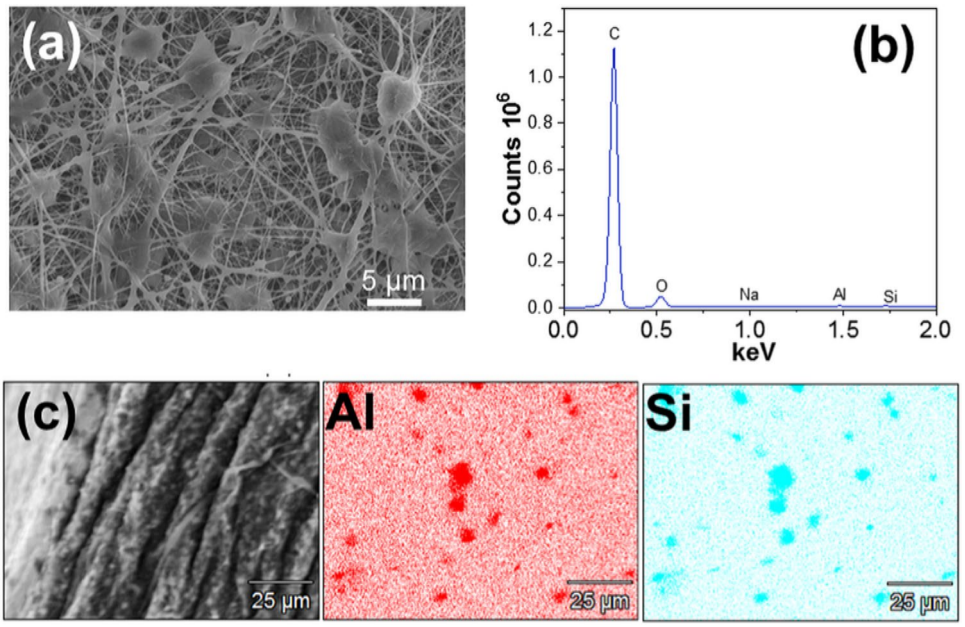

Fig. 6 **a** SEM image of PPF (**b**), EDS-SEM spectrum of PPF (**c**), EDS-SEM image Al and Si detection elements

The PP 10 fiber membranes results showed the best combination of the PCL and PEC polymers, being the choice as the polymeric matrix for FAU zeolite insertion. FAU particulate 2.5% (w w^{-1}) was evaluated to improve the mechanical properties of the PP 10 membrane. In Fig. 6a, it is possible to observe that in PPF, a formation of PEC regions with good homogeneity in all polymeric surfaces. Thus, the FAU presence could be contributed as hydrophilic material to establish PEC polymer, increasing their dispersion, which was not previously observed in Fig. 2b–e for PP blends.

The EDS-SEM spectrum in Fig. 6c shows a composition of PPF fiber membranes, making it possible to check the presence of atomic elements Si, Al, and Na from FAU zeolite. The highest count of C element is relative to both chain polymers that form the fiber membranes. The EDS-SEM image (Fig. 6d) also suggests FAU disperses with agglomeration in the PPF membrane. Hence, PPF mechanical results showed that FAU insertion turns the membrane more resistant to manipulation and break, an essential property of wound dressing.

In Fig. 7a, it is verified PCL and PP 10 traction resistance values of 0.46 ± 0.07 and 0.63 ± 0.03, respectively. The average strain at fracture corresponds to 7.6 ± 0.5 and 6.1 ± 0.5 for PCL and PP 10, respectively. These results show that while FAU increases the tensile strength at fracture, the deformation capacity of fibers is impaired, and they can break more easily. Adding FAU in the PP 10 blend allows the nanocomposite PPF to have a superior stress value of 3.1 ± 0.3 MPa and strain deformation of 5.5 ± 0.4%. This higher resistance of traction in PPF by FAU insertion is due to the possible intercalation between polymeric chains, which is necessary for a more potent force to rupture the membrane. The result corroborates with the literature [60, 61] that particulates intercalated in polymeric matrix improve the stress resistance.

Another favorable contribution of FAU insertion in PPF nanocomposite is the hydrophilicity with the value of angle contact corresponding to 97 ± 19°. The value found is inferior to PP 10 (104 ± 5°). Thus, the incorporation of lower FAU

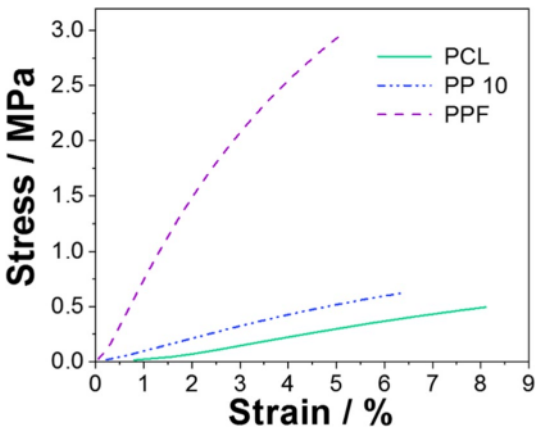

Fig. 7 Mechanical behavior of PPF fiber membranes

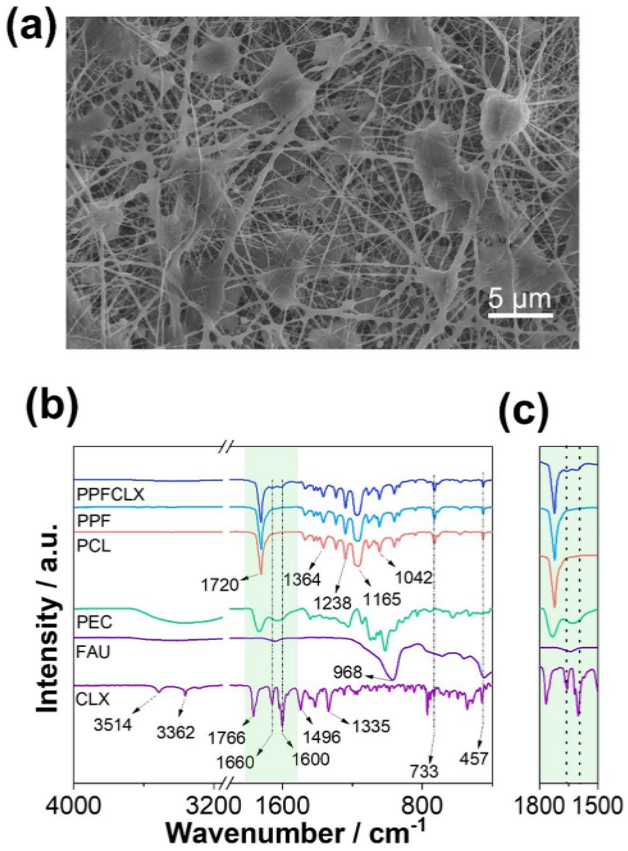

Fig. 8 SEM image of PPFCLX sample (**a**), FTIR structural analysis (**b**), and high magnification of the FTIR spectra to CLX detection region (**c**)

(2.5%) resulted in a considerable increase in the material's hydrophilicity to the ability of the zeolite, containing silanol groups, allowing it to interact and keep water trapped in its 3D cavity. The same behavior was observed in other studies, as reported in the literature [62] using polymer fibers reinforced with zeolite. Hence, the PPF fiber membranes improved the properties of wound dressing material by individual characteristics.

3.3 Antimicrobial and drug release—PPFCLX

PPF membranes were used to support the addition of cloxacillin (CLX) as an antibiotic model to be evaluated against their antimicrobial activity and drug release. Initially, the SEM image of PPFCLX (Fig. 8a) exhibits the fiber formation presence of beads of varying dimensions and randomly distributed in the fibers, as previously verified to PPF in Fig. 6a. Thus, the CLX immobilization in the structure of the polymeric fibers did not affect the membrane morphology.

FTIR analysis (Fig. 8b) exhibited only the typical bands of PCL in PPF fiber membranes according to the literature [63–66], masking the PEC and FAU presence because of their intense vibrations. PCL has a doublet between 2800 and 3000 cm^{-1}, corresponding to the symmetrical and asymmetrical stretching of the C-H bonds of the methylene group. The band at 1720 cm^{-1} corresponds to the vibrations of the carbonyl (C=O) present in the PCL structure, while the bands at 1238 and 1165 cm^{-1} refer, respectively, to the asymmetric and symmetric stretching of the C–O–C bond. The bands referring to PEC are located at 3362 cm^{-1}, referring to the stretching of OH groups, and the bands near 2934 and 1496 cm^{-1} correspond to the deformation of CH_2 groups [67]. The signal at 1720 cm^{-1} also represents vibrations of the carbonyl group present in the PEC, those at 1600 and 1410 cm^{-1} indicate asymmetric and symmetric stretching of the COO^- group, respectively. The vibrations of the C-O group are shown in the 1238 and 968 cm^{-1} bands, the asymmetric stretching of the O–C–O bond appears at 1142 cm^{-1}, and both the C–C and C–O groups vibrate in other regions. The absence of detection may be because the most intense bands in the spectrum of PEC and PCL are related to groups that vibrate in the overlapping areas (C=O, C–O, C–C, and C–H). For zeolite, observed bands in the 3700–3100 cm^{-1} region are related to the presence of OH^- anions in the structure, and a band in the 1660 cm^{-1} region is associated with the vibration of water hydration molecules [68].

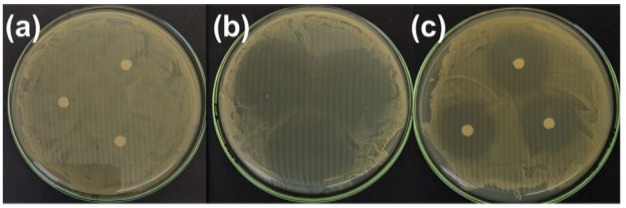

Fig. 9 Inhibition halo assay for antimicrobial activity against *S. aureus* bacteria in **a** PPF, **b** CLX-free drug, and **c** PPFCLX

Additionally, it is possible to observe the presence of bands at 457 cm^{-1} referring to the bending of the internal TO_4 tetrahedra (T = Si, Al) and at 570–560 cm^{-1} associated with the bonding of the external double rings. These spectra also show bands at 690–680 cm^{-1} related to the symmetrical stretching of external bonds, while at 780–770 cm^{-1}, they are associated with the symmetrical stretching of 4-membered rings. The bands at 990–970 cm^{-1} are related to the asymmetric stretching of the internal tetrahedra. The two most intense vibrational modes of FAU, at 970 and 457 cm^{-1}, are related to the Si–O bond, coinciding with PCL's broad and intense vibrational modes.

The spectrum for cloxacillin in Fig. 8b reveals the presence of bands directly related to the structure of the drug. At 3514 cm^{-1}, a prominent band is observed, referring to the presence of water molecules. In contrast, the band at 33,620 cm^{-1} indicates the stretching of the N–H bond. The band at 1766 cm^{-1} is related to the beta-lactam's carbonyl, while the secondary amide's carbonyl absorbs at 1660 cm^{-1}. The bands at 1619 and 750 cm^{-1} refer to the aromatic ring, while those at 1600, 1414, and 1335 cm^{-1} are associated with the carboxylate ion. The C=N, N–O, N–C, and C–O bonds are represented by the bands at 1496, 1294, 1213 and 1128 cm^{-1}, respectively. The spectrum agrees with the literature [69, 70]. In the PPFCLX spectrum, it was possible to verify bands of cloxacillin between 1598 and 1665 cm^{-1}, demonstrating the drug incorporation in the membrane. The infrared spectra have overlapping bands for the different structures, but they all prove their presence.

In the antimicrobial assays, initially, negative control of the PPF composite without the presence of CLX was maintained in the presence of the bacteria *S. aureus* by time of 12 h at 36 °C (Fig. 9a). The results show that bacterial growth in the presence of PPF was not inhibited, confirming that PCL, PEC and FAU have no bacterial activity. A positive control with CLOX alone was also carried out to assess the inhibition of bacterial growth. Bactericidal activity was confirmed by an inhibition halo with an enlarged diameter (Fig. 9b). This result was achieved due to the ease with which the antibiotic diffuses into the culture medium when added in its free form. The inhibition of the growth of the *S. aureus* bacteria was also confirmed when the PPFCLX composite was inoculated with the bacteria (Fig. 9c). An inhibition halo of 28 mm was achieved symmetrically around the small PPFCLX spheres. This result allows us to conclude that the antibiotic was successfully immobilized in the composite and its release into the culture medium was not impaired, given the extent of the inhibition halo. The evidence of bactericidal activity shows the composite's potential for application as a wound dressing. Its use inhibits the proliferation of *S. Aureus* in regions close to the application site and can accelerate wound healing. This prolonged bactericidal activity can be achieved by maintaining adequate concentrations of the antibiotic at the application site. Thus, confirming the release of the drug over time is a result of interest for medical applications which was also investigated in this study.

CLX drug release was performed at underbody temperature (37 °C), constant stirring in ultrapure water (pH 6.6), PO_4^{3-} and CO_3^{2-} buffer solutions (pH 5.5), simulating human-biological environments. CLX molecule has a water solubility of 53 mg L^{-1} and pKa equal to 2.78, presented in its deprotonated form. In Fig. 10a, it is possible to observe that initially, the CLX is quickly released from PPFCLX. Still, the drug concentration decreased in sequence, especially by water medium. This result can be attributed to the competitive release process and readsorption of CLX by membrane. Once the experimental medium allows the drug accumulation, dynamic transference does not occur. The released CLX in the simulated experiment was not consumed by any process being re-absorbed by the PPFCLX. In the biological process, the available drug is absorbed by skin cells, and its concentration in the body fluids is replenished continuously. This result indicates the affinity of the cloxacillin drug with the PPF membrane. In the literature [71, 72], membranes are usually applied to remediate contaminant molecules, including drugs. Differences in the adsorption of CLX can be associated with the stability of the drug in suspension by electrostatic or Van der Waals interaction [73, 74]. A higher decrease in the water medium was observed, followed by PO_4^{3-} and CO_3^{2-} buffer.

The release behavior in Fig. 10b exhibits a maximum value available that was less than the 1 h of exposition. The CLX concentrations reached were 5.56 ± 0.01 mg L^{-1} in water, 6.18 ± 0.02 mg L^{-1} in PO_4^{3-} buffer, and 1.21 ± 0.10 mg L^{-1} in CO_3^{2-} buffer (Fig. 10b). Additionally, the plateau found were kept stable until 10 h evaluated, indicating the maximum amount released in the experimental condition. In the case of CO_3^{2-} buffer, this one shows its instability, involved in a dynamic process forming CO_2 gas [75]. The exciting thing about the CO_3^{2-} buffer is the simulation of internal body fluids

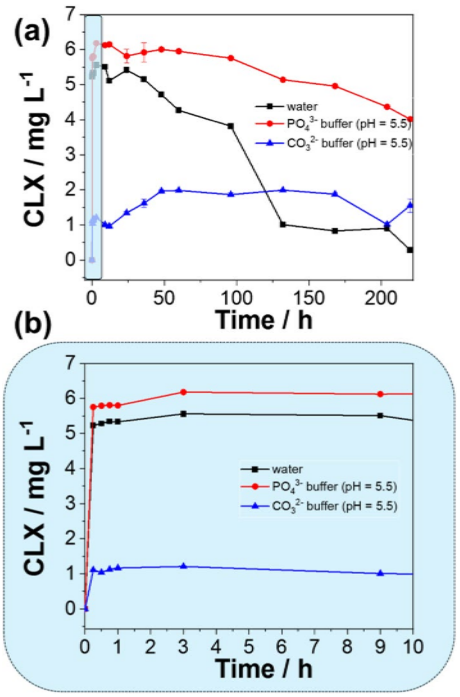

Fig. 10 **a** CLX drug release from PPFCLX fiber membranes in different conditions for 239 h, and **b** high magnification of the initial region (until 10 h)

and the gastrointestinal system. However, CO_2 formation induces pH instability and bubbles formation, affecting the drug dissolution and the diffusion layer close to the surface of the delivery system [76]. Thus, the ion effect of CO_3^{2-} and PO_4^{3-} buffer (Fig. 10b) in CLX release demonstrated the importance of the external parameters as buffer characteristics: type, capacity, and ionic strength are essential to the releasing behavior [77].

Hence, the results prove that the PPFCLX can release CLX by transferring it from the membrane to an external medium, indicating that it is an alternative material to be a drug carrier. Thus, the release results associated with the bactericidal activity (Fig. 9) demonstrate that CLX was efficiently immobilized. The nanocomposite can be applied as a potential drug delivery to wound dressing, helping to heal and control the proliferation of microorganisms.

4 Conclusions

This work developed PPFCLX nanocomposite fibers by electrospinning, containing the cloxacillin antibiotic for application as a controlled-release antimicrobial membrane. The PEC addiction in PP fibers showed hydrophobic properties and stable degradability in phosphate buffer conditions simulating human skin pH (5.5). These results are attributed to the lower PEC amount of blended PCL, even with 10% (w w^{-1}) added to the initial polymeric solution. PPF fibers inserting 2.5% FAU resulted in membranes with better tensile strength properties. The nanocomposite PCL:PEC:FAU (PPF) with 2.5 (w w^{-1}) insertion increased the resistance to fracture from 0.63 ± 0.03 to 3.1 ± 0.3 MPa, exhibiting a better mechanical response. The CLX (20%) antimicrobial properties were proven from *Staphylococcus aureus* (Gram-positive) growth inhibition assays. Furthermore, simulating temperature (37 °C) and cell pH in the CLX release assays with different solutions (water, PO_4^{3-} or CO_3^{2-} buffer, pH equal to 5.5 and 5 mmol L^{-1}). A continuous releasing of CLX exhibited in the first 3 h for water (5.56 ± 0.01 mg L^{-1}) and the PO_4^{3-} buffer (6.18 ± 0.02 mg L^{-1}) superior values than found in the CO_3^{2-} (1.21 ± 0.10 mg L^{-1}), maintained constant during until 10 h. In this way, the system proposed that PPF presented desirable properties such as greater hydrophobicity, resistance to traction, bactericidal activity, and antibiotic release, showing potential material such as membranes for wounds.

Acknowledgements This study was financed in part by the Coordenação de Aperfeiçoamento de Pessoal de Nível Superior—Brasil (CAPES)—Finance Code 001. FAPESP (Grant Number 2019/23412-9, 2021/14992-1, 2022/06219-3, 2023/17483-6, 2023/03632-0). For financial support, the authors acknowledge Embrapa (Grant Number 11.14.03.001.01.00), FINEP, SisNano, and AgroNano Network.

Author contributions B. B. writing and methodology; J. O. D. M.: writing, editing, and conceptualization; A. J. M. writing, editing, and methodology; A. C. A.N., J. B. L. methodology; L. A. F. V. editing and methodology; E. C. P.:conceptualization, supervision and review; All authors reviewed the manuscript.

Data availability The data that support the findings of this study are available from the corresponding author upon reasonable request.

Declarations

Competing interests The authors declare no competing interests.

References

1. Nguyen HM, Le Ngoc TT, Nguyen AT, et al. Biomedical materials for wound dressing: recent advances and applications. RSC Adv. 2023;13:5509–28. https://doi.org/10.1039/d2ra07673j.
2. Schneider R, Mercante LA, Andre RS, et al. Biocompatible electrospun nanofibers containing cloxacillin: antibacterial activity and effect of pH on the release profile. React Funct Polym. 2018;132:26–35. https://doi.org/10.1016/j.reactfunctpolym.2018.09.001.
3. Kim HS, Sun X, Lee JH, et al. Advanced drug delivery systems and artificial skin grafts for skin wound healing. Adv Drug Deliv Rev. 2019;146:209–39. https://doi.org/10.1016/j.addr.2018.12.014.
4. Chin JS, Madden L, Chew SY, Becker DL. Drug therapies and delivery mechanisms to treat perturbed skin wound healing. Adv Drug Deliv Rev. 2019;149–150:2–18. https://doi.org/10.1016/j.addr.2019.03.006.
5. Grabsk AHA, de Souza JRB, De Marchi FE, et al. Determination of antibiotics residues in milk using a QuECHERS method using full factorial design and liquid chromatography-tandem mass spectrometry. J Braz Chem Soc. 2019;30:1498–505. https://doi.org/10.21577/0103-5053.20190046.
6. Touza-Otero L, Landin M, Diaz-Rodriguez P. Fighting antibiotic resistance in the local management of bovine mastitis. Biomed Pharmacother. 2024;170:115967–76. https://doi.org/10.1016/j.biopha.2023.115967.
7. Sadeghianmaryan A, Ahmadian N, Wheatley S, et al. Advancements in 3D-printable polysaccharides, proteins, and synthetic polymers for wound dressing and skin scaffolding: a review. Int J Biol Macromol. 2024;266:131207–27. https://doi.org/10.1016/j.ijbiomac.2024.131207.
8. Hegde V, Uthappa UT, Altalhi T, et al. Alginate based polymeric systems for drug delivery, antibacterial/microbial, and wound dressing applications. Mater Today Commun. 2022;33:104813–34. https://doi.org/10.1016/j.mtcomm.2022.104813.
9. Winzenburg G, Schmidt C, Fuchs S, Kissel T. Biodegradable polymers and their potential use in parenteral veterinary drug delivery systems. Adv Drug Deliv Rev. 2004;56:1453–66. https://doi.org/10.1016/j.addr.2004.02.008.
10. Gruppuso M, Turco G, Marsich E, Porrelli D. Polymeric wound dressings, an insight into polysaccharide-based electrospun membranes. Appl Mater Today. 2021;24:101148–90. https://doi.org/10.1016/j.apmt.2021.101148.
11. Parın FN, Ullah A, Yeşilyurt A, et al. Development of PVA–psyllium husk meshes via emulsion electrospinning: preparation, characterization, and antibacterial activity. Polymers (Basel). 2022;14:1490–505. https://doi.org/10.3390/polym14071490.
12. Malafatti JOD, Bernardo MP, Moreira FKV, et al. Electrospun poly(lactic acid) nanofibers loaded with silver sulfadiazine/[Mg–Al]-layered double hydroxide as an antimicrobial wound dressing. Polym Adv Technol. 2020;31:1377–87. https://doi.org/10.1002/pat.4867.
13. de Jesus ET, Moreira AJ, Sá MC, et al. Potential of Nb2O5 nanofibers in photocatalytic degradation of organic pollutants. Environ Sci Pollut Res. 2021;28:69401–15. https://doi.org/10.1007/s11356-021-15435-8.
14. Parın FN, Ullah S, Yıldırım K, et al. Fabrication and characterization of electrospun folic acid/hybrid fibers: In vitro controlled release study and cytocompatibility assays. Polymers (Basel). 2021;13:3594–614. https://doi.org/10.3390/polym13203594.
15. Parın FN, Aydemir Çİ, Taner G, Yıldırım K. Co-electrospun-electrosprayed PVA/folic acid nanofibers for transdermal drug delivery: preparation, characterization, and in vitro cytocompatibility. J Ind Text. 2022;51:1323S-1347S. https://doi.org/10.1177/1528083721997185.
16. Villarino N, Landoni MF. Transdermal drug delivery: a new frontier in the administration of therapeutic drugs to veterinary species. Vet J. 2006;172:200–1. https://doi.org/10.1016/j.tvjl.2005.09.009.
17. Riviere JE, Papich MG. Potential and problems of developing transdermal patches for veterinary applications. Adv Drug Deliv Rev. 2001;50:175–203. https://doi.org/10.1016/S0169-409X(01)00157-0.
18. Hamzah MSA, Austad A, Razak SIA, Nayan NHM. Tensile and wettability properties of electrospun polycaprolactone coated with pectin/polyaniline composite for drug delivery application. Int J Struct Integr. 2019;10:704–13. https://doi.org/10.1108/IJSI-04-2019-0033.
19. Thakur BR, Singh RK, Handa AK. Chemistry and uses of pectin: a review. Crit Rev Food Sci Nutr. 1997;37:47–73. https://doi.org/10.1080/10408399709527767.

20. Yang Z, Peng H, Wang W, Liu T. Crystallization behavior of poly(ε-caprolactone)/layered double hydroxide nanocomposites. J Appl Polym Sci. 2010;116:2658–67. https://doi.org/10.1002/app.
21. Shabeena M, Warale D, Prabhu A, et al. Pectin wrapped halloysite nanotube reinforced Polycaprolactone films for potential wound healing application. Int J Biol Macromol. 2024;262:130140–56. https://doi.org/10.1016/j.ijbiomac.2024.130140.
22. Fu SY, Feng XQ, Lauke B, Mai YW. Effects of particle size, particle/matrix interface adhesion and particle loading on mechanical properties of particulate-polymer composites. Compos Part B Eng. 2008;39:933–61. https://doi.org/10.1016/j.compositesb.2008.01.002.
23. Bhardwaj I, Saini N, Devi M, Kataria R. Biomaterials for drug delivery. Encycl Green Mater. 2023. https://doi.org/10.1007/978-981-16-4921-9_152-1.
24. Shavisi N. Electrospun fiber mats based on chitosan-carrageenan containing Malva sylvestris anthocyanins: physic-mechanical, thermal, and barrier properties along with application as intelligent food packaging materials. Int J Biol Macromol. 2024;266:131077–87. https://doi.org/10.1016/j.ijbiomac.2024.131077.
25. Yavari Maroufi L, Ghorbani M, Mohammadi M, Pezeshki A. Improvement of the physico-mechanical properties of antibacterial electrospun poly lactic acid nanofibers by incorporation of guar gum and thyme essential oil. Colloids Surfaces A Physicochem Eng Asp. 2021;622:126659–67. https://doi.org/10.1016/j.colsurfa.2021.126659.
26. Vergara-Figueroa J, Alejandro-Martin S, Cerda-Leal F, Gacitúa W. Dual electrospinning of a nanocomposites biofilm: Potential use as an antimicrobial barrier. Mater Today Commun. 2020;25:101671–82. https://doi.org/10.1016/j.mtcomm.2020.101671.
27. Malafatti JOD, Tavares FA, Neves TR, et al. Modified silica nanoparticles from rice husk supported on polylactic acid as adsorptive membranes for dye removal. Materials (Basel). 2023;16:2429–46. https://doi.org/10.3390/ma16062429.
28. Ribeiro AS, Costa SM, Ferreira DP, et al. Chitosan/nanocellulose electrospun fibers with enhanced antibacterial and antifungal activity for wound dressing applications. React Funct Polym. 2021;159:104808–17. https://doi.org/10.1016/j.reactfunctpolym.2020.104808.
29. Ferreira CAM, Guerreiro SFC, Valente JFA, et al. Advanced face mask filters based on PCL electrospun meshes dopped with antimicrobial MgO and CuO nanoparticles. Polymers (Basel). 2022;14:3329–46. https://doi.org/10.3390/polym14163329.
30. Bulbul YE, Okur M, Demirtas-Korkmaz F, Dilsiz N. Development of PCL/PEO electrospun fibrous membranes blended with silane-modified halloysite nanotube as a curcumin release system. Appl Clay Sci. 2020;186:105430–43. https://doi.org/10.1016/j.clay.2019.105430.
31. Khodaverdi E, Soleimani HA, Mohammadpour F, Hadizadeh F. Synthetic zeolites as controlled-release delivery systems for anti-inflammatory drugs. Chem Biol Drug Des. 2016;87:849–57. https://doi.org/10.1111/cbdd.12716.
32. Paris EC, Malafatti JOD, Musetti HC, et al. Faujasite zeolite decorated with cobalt ferrite nanoparticles for improving removal and reuse in Pb2+ ions adsorption. Chin J Chem Eng. 2020;28:1884–90. https://doi.org/10.1016/j.cjche.2020.04.019.
33. Lopes MM, Coutinho TC, Malafatti JOD, et al. Immobilization of phytase on zeolite modified with iron(II) for use in the animal feed and food industry sectors. Process Biochem. 2021;100:260–71. https://doi.org/10.1016/j.procbio.2020.10.017.
34. Ninan N, Muthiah M, Park IK, et al. In vitro and in vivo evaluation of pectin/copper exchanged faujasite composite membranes. J Biomed Nanotechnol. 2015;11:1550–67. https://doi.org/10.1166/jbn.2015.2098.
35. Iqbal N, Abdul-Kadir MR, Mahmood NHB, et al. Microwave synthesis, characterization, bioactivity and in vitro biocompatibility of zeolite-hydroxyapatite (Zeo-HA) composite for bone tissue engineering applications. Ceram Int. 2014;40:16091–7. https://doi.org/10.1016/j.ceramint.2014.07.038.
36. Parin FN, Terzioğlu P, Sicak Y, et al. Pine honey–loaded electrospun poly (vinyl alcohol)/gelatin nanofibers with antioxidant properties. J Text Inst. 2021;112:628–35. https://doi.org/10.1080/00405000.2020.1773199.
37. Basar AO, Castro S, Torres-Giner S, et al. Novel poly(ε-caprolactone)/gelatin wound dressings prepared by emulsion electrospinning with controlled release capacity of Ketoprofen anti-inflammatory drug. Mater Sci Eng C. 2017;81:459–68. https://doi.org/10.1016/j.msec.2017.08.025.
38. Ustundag CR, Piskin MB. Investigation of electrospun poly (ε-caprolactone) fiber mats loaded with Calophyllum inophyllum essential oil for wound dressing applications: morphology, drug release and in vitro evaluation. Mater Technol. 2023;38:2223018–3222332. https://doi.org/10.1080/10667857.2023.2223018.
39. Hosseini SA, Javad Hoseini S, Askari VR, et al. Pectin-reinforced electrospun nanofibers: Fabrication and characterization of highly biocompatible mats for wound healing applications. J Drug Deliv Sci Technol. 2022;77:103916–26. https://doi.org/10.1016/j.jddst.2022.103916.
40. Alipour M, Aghazadeh M, Akbarzadeh A, et al. Towards osteogenic differentiation of human dental pulp stem cells on PCL-PEG-PCL/zeolite nanofibrous scaffolds. Artif Cells Nanomed Biotechnol. 2019;47:3431–7. https://doi.org/10.1080/21691401.2019.1652627.
41. Sarvari R, Nouri M, Roshangar L, et al. Conductive bio-copolymers based on pectin-polycaprolactone/ polyaniline and tissue engineering application thereof. J Ultrafine Grained Nanostruct Mater. 2021;54:64–72. https://doi.org/10.22059/jufgnsm.2021.01.07.
42. Wang J, Windbergs M. Functional electrospun fibers for the treatment of human skin wounds. Eur J Pharm Biopharm. 2017;119:283–99. https://doi.org/10.1016/j.ejpb.2017.07.001.
43. Yuan Y, Choi K, Choi SO, Kim J. Early stage release control of an anticancer drug by drug-polymer miscibility in a hydrophobic fiber-based drug delivery system. RSC Adv. 2018;8:19791–803. https://doi.org/10.1039/c8ra01467a.
44. Silva EC, Oliveira TJ, Moreli FC, et al. Newly isolated lytic bacteriophages for Staphylococcus intermedius, structurally and functionally stabilized in a hydroxyethylcellulose gel containing choline geranate: potential for transdermal permeation in veterinary phage therapy. Res Vet Sci. 2021;135:42–58. https://doi.org/10.1016/j.rvsc.2020.12.013.
45. Amna T, Shamshi Hassan M, Pandurangan M, et al. Characterization and potent bactericidal effect of Cobalt doped Titanium dioxide nanofibers. Ceram Int. 2013;39:3189–93. https://doi.org/10.1016/j.ceramint.2012.10.003.
46. Meirelles MR, Malafatti JOD, Escote MT, et al. Magnetic adsorbent based on faujasite zeolite decorated with magnesium ferrite nanoparticles for metal ion removal. Magnetochemistry. 2023;9:136–49. https://doi.org/10.3390/magnetochemistry9050136.
47. Malafatti JOD, Machado T, Ruellas DO, et al. PLA / starch biodegradable fibers obtained by the electrospinning method for micronutrient mineral release. AIMS Mater Sci. 2023;10:200–12. https://doi.org/10.3934/matersci.2023011.
48. Costa RGF, de Oliveira JE, de Paula GF, et al. Eletrofiação de Polímeros em Solução: parte I: fundamentação TeÃ³rica. Polímeros. 2012;22:170–7. https://doi.org/10.1590/S0104-14282012005000026.
49. Ameri A, Faramarzi MA, Tarighi S, et al. Removal of dyes by Trametes versicolor laccase immobilized on NaY-zeolite. Chem Eng Res Des. 2023;197:240–53. https://doi.org/10.1016/j.cherd.2023.07.014.

50. Ghojavand S, Dib E, Mintova S. Flexibility in zeolites: origin, limits, and evaluation. Chem Sci. 2023;14:12430–46. https://doi.org/10.1039/d3sc03934j.
51. Osada M, Sasaki I, Nishioka M, et al. Synthesis of a faujasite thin layer and its application for SO2 sensing at elevated temperatures. Microporous Mesoporous Mater. 1998;23:287–94. https://doi.org/10.1016/S1387-1811(98)00125-5.
52. Azizi SN, Alavi Daghigh A, Abrishamkar M. Phase transformation of zeolite P to y and analcime zeolites due to changing the time and temperature. J Spectrosc. 2013;1:428216–20. https://doi.org/10.1155/2013/428216.
53. Srikanth B, Goutham R, Badri Narayan R, et al. Recent advancements in supporting materials for immobilised photocatalytic applications in waste water treatment. J Environ Manag. 2017;200:60–78. https://doi.org/10.1016/j.jenvman.2017.05.063.
54. Abdulkadir BA, Mohd Zaki RSR, Abd Wahab AT, et al. A concise review on surface and structural modification of porous zeolite scaffold for enhanced hydrogen storage. Chin J Chem Eng. 2024;70:33–53. https://doi.org/10.1016/j.cjche.2024.03.001.
55. Liu Z, Shi C, Wu D, et al. A simple method of preparation of high silica zeolite y and its performance in the catalytic cracking of cumene. J Nanotechnol. 2016;1:1486107–12. https://doi.org/10.1155/2016/1486107.
56. Gueci L, Ferrante F, Bertini M, et al. DFT study on zeolites' intrinsic Brønsted acidity: the case of BEA. Comput Mater Sci. 2024;232:112687–95. https://doi.org/10.1016/j.commatsci.2023.112687.
57. Zhu Z, Troemner M, Wang W, et al. Lattice discrete particle modeling of the cycling behavior of strain-hardening cementitious composites with and without fiber reinforced polymer grid reinforcement. Compos Struct. 2023;322:117346–58. https://doi.org/10.1016/j.compstruct.2023.117346.
58. Gaikwad D, Sutar R, Patil D. Polysaccharide mediated nanodrug delivery: a review. Int J Biol Macromol. 2024;261:129547–66. https://doi.org/10.1016/j.ijbiomac.2024.129547.
59. Lavy E, Kirmayer D, Nudelman Z, et al. Aspects in controlled drug delivery for topical applications in veterinary medicine. Vet Anim Sci. 2022;15:100235. https://doi.org/10.1016/j.vas.2022.100235.
60. Wang H, Xu H, Li H, et al. Electrospun polyurethane/zeolitic imidazolate framework nanofibrous membrane with superior stability for filtering performance. ACS Appl Polym Mater. 2021;3:710–9. https://doi.org/10.1021/acsapm.0c01005.
61. Bahi A, Shao J, Mohseni M, Ko FK. Membranes based on electrospun lignin-zeolite composite nanofibers. Sep Purif Technol. 2017;187:207–13. https://doi.org/10.1016/j.seppur.2017.06.015.
62. Kang DH, Kang HW. Surface energy characteristics of zeolite embedded PVDF nanofiber films with electrospinning process. Appl Surf Sci. 2016;387:82–8. https://doi.org/10.1016/j.apsusc.2016.06.096.
63. Phillipson K, Hay JN, Jenkins MJ. Thermal analysis FTIR spectroscopy of poly(ε-caprolactone). Thermochim Acta. 2014;595:74–82. https://doi.org/10.1016/j.tca.2014.08.027.
64. Chong LH, Lim MM, Sultana N. Fabrication and evaluation of polycaprolactone/gelatin-based electrospun nanofibers with antibacterial properties. J Nanomater. 2015;1:970542–9. https://doi.org/10.1155/2015/970542.
65. Abderrahim B, Abderrahman E, Mohamed A, et al. Kinetic thermal degradation of cellulose, polybutylene succinate and a green composite: comparative study. World J Environ Eng. 2015;3:95–110. https://doi.org/10.12691/WJEE-3-4-1.
66. Aragón J, Costa C, Coelhoso I, et al. Electrospun asymmetric membranes for wound dressing applications. Mater Sci Eng C. 2019;103:109822–33. https://doi.org/10.1016/j.msec.2019.109822.
67. Szymanska-Chargot M, Zdunek A. Use of FT-IR spectra and PCA to the bulk characterization of cell wall residues of fruits and vegetables along a fraction process. Food Biophys. 2013;8:29–42. https://doi.org/10.1007/s11483-012-9279-7.
68. Król M, Mozgawa W, Jastrzbski W, Barczyk K. Application of IR spectra in the studies of zeolites from D4R and D6R structural groups. Microporous Mesoporous Mater. 2012;156:181–8. https://doi.org/10.1016/j.micromeso.2012.02.040.
69. Mays DL. Cloxacillin sodium. Anal Profiles Drug Subst Excipients. 1975;4:113–36. https://doi.org/10.1016/S0099-5428(08)60010-6.
70. Chao JB, Xu MD, Yin CX, Huang S. Synthesis of Zn(II)–cloxacillin sodium complex and study of its interaction with calf thymus DNA. Russ Biokhimiya. 2007;72:184–93. https://doi.org/10.1134/S0006297907020046.
71. Mascarenhas BC, Tavares FA, Paris EC. Functionalized faujasite zeolite immobilized on poly(lactic acid) composite fibers to remove dyes from aqueous media. J Appl Polym Sci. 2020;137:1–12. https://doi.org/10.1002/app.48561.
72. Alp-Erbay E, Figueroa-Lopez KJ, Lagaron JM, et al. The impact of electrospun films of poly(ε-caprolactone) filled with nanostructured zeolite and silica microparticles on in vitro histamine formation by *Staphylococcus aureus* and Salmonella Paratyphi A. Food Packag Shelf Life. 2019;22:100414–26. https://doi.org/10.1016/j.fpsl.2019.100414.
73. de Oliveira C, Renda CG, Moreira AJ, et al. Evaluation of a graphitic porous carbon modified with iron oxides for atrazine environmental remediation in water by adsorption. Environ Res. 2023;219:115054–65. https://doi.org/10.1016/j.envres.2022.115054.
74. Renda CG, Contreras Medrano CP, Costa LJD, et al. Role of ferrocene-derived iron species in the catalytic graphitization of novolak resins. J Mater Sci. 2021;56:1298–311. https://doi.org/10.1007/s10853-020-05312-z.
75. Ikuta S, Nakagawa H, Kai T, Sugano K. Development of bicarbonate buffer flow-through cell dissolution test and its application in prediction of in vivo performance of colon targeting tablets. Eur J Pharm Sci. 2023;180:106326–33. https://doi.org/10.1016/j.ejps.2022.106326.
76. Broesder A, Woerdenbag HJ, Prins GH, et al. pH-dependent ileocolonic drug delivery, part I: in vitro and clinical evaluation of novel systems. Drug Discov Today. 2020;25:1362–73. https://doi.org/10.1016/j.drudis.2020.06.011.
77. Krollik K, Lehmann A, Wagner C, et al. The effect of buffer species on biorelevant dissolution and precipitation assays: comparison of phosphate and bicarbonate buffer. Eur J Pharm Biopharm. 2022;171:90–101. https://doi.org/10.1016/j.ejpb.2021.09.009.